



Search for WH Production Using The Matrix Element Analysis Technique in 900 pb^{-1} of Data Collected with the DØ Detector

The DØ Collaboration
URL <http://www-d0.fnal.gov>

(Dated: March 15, 2007)

This note describes the application of the matrix element analysis technique to the search for WH production at DØ using approximately 900 pb^{-1} of Run II data. From a comparison of the matrix element discriminants between data and the background model, we set an upper limit on the production cross section for WH events as a function of the mass of the Higgs boson. For a Higgs boson mass of $115 \text{ GeV}/c^2$ we arrive at a 95% CL upper limit of:

$$\sigma_{WH} \times BR(H \rightarrow b\bar{b}) \leq 1.74 \text{ pb} \quad (\leq 1.20 \text{ pb expected}).$$

Preliminary Results for Winter 2007 Conferences

I. INTRODUCTION

The most sensitive search channel at the Tevatron for a Higgs boson with a mass below approximately $130 \text{ GeV}/c^2$ is for a Higgs boson produced in association with a W boson. For $m_H < 130 \text{ GeV}/c^2$ the dominant Higgs decay mode is $H \rightarrow b\bar{b}$. This note reports on a search for a Higgs boson in the $e\nu b\bar{b}$ (e +jets) and the $\mu\nu b\bar{b}$ (μ +jets) final states using the Matrix Element technique to separate signal from background. We only consider events with exactly two jets, at least one of which has to be b -tagged. Events are treated separately throughout the analyses depending on the lepton flavor and the number of b -tagged jets they contain. We consider four independent channels: e +jets/1-tag, e +jets/2-tag, μ +jets/1-tag and μ +jets/2-tag. The signal-to-background ratio is significantly different for single and double tagged events and the sensitivity is increased by treating them as independent channels. This also allows for a separate optimization of the WH discriminant in each channel. Finally, the four independent channels are combined in the limit setting step of the analysis.

II. DØ DETECTOR

The DØ Run II detector [1, 2] consists of the following main components: a central tracking system, a liquid-argon/uranium calorimeter, and a muon spectrometer.

The central tracking system includes a silicon microstrip tracker (SMT) and a central fiber tracker (CFT), both located in a 2 T superconducting solenoid magnet. The SMT is designed to provide efficient tracking and vertexing capability at pseudorapidities of $|\eta| < 3$. The SMT has a six-barrel longitudinal structure, each with a set of four layers arranged axially around the beam pipe, and interspersed with 16 radial disks. A typical pitch of 50-80 μm of the silicon strips allows a precision determination of the three-dimensional track impact parameter with respect to the primary vertex which is the key component of the lifetime based b -jet tagging algorithms. The CFT has eight coaxial barrels, each supporting two doublets of overlapping scintillating fibers of 0.835 mm diameter, one doublet being parallel to the collision axis, and the other alternating by $\pm 3^\circ$ relative to the axis.

The calorimeter is divided into a central section (CC) providing coverage out to $|\eta| \approx 1$, and two end calorimeters (EC) extending coverage to $|\eta| \approx 4$, all housed in separate cryostats. Scintillators placed between the CC and EC provide sampling of showers at $1.1 < |\eta| < 1.4$.

The muon system, covering pseudorapidities of $|\eta| < 2$, resides beyond the calorimetry, and consists of three layers of tracking detectors and scintillating trigger counters. Moving radially outwards, the first layer is placed before the 1.8 T toroid magnets, and the two following layers are located after the magnets.

III. SIMULATED EVENT SAMPLES

The WH signal was generated with the PYTHIA [3] Monte Carlo event generator. The Higgs boson was forced to decay to $b\bar{b}$ and separate samples for $W \rightarrow e\nu$, $W \rightarrow \mu\nu$, $W \rightarrow \tau\nu$, were generated. Hadrons containing b quarks were decayed using EvtGen [4].

To estimate the backgrounds, the following samples were generated: W +jets, including $W+cc$, $W+cj$ and $W+bb$, and $t\bar{t}$ samples were generated using ALPGEN [5], WW and WZ samples were generated using PYTHIA, and single top samples were generated with the CompHEP-SingleTop [6] Monte Carlo event generator.

For all samples, the set of parton distribution functions used is CTEQ6L1 [7], and the top quark mass is set to $175 \text{ GeV}/c^2$.

IV. DATA SAMPLE AND EVENT SELECTION

The analysis is based on data collected between August 2002 and December 2005, with triggers that required a jet and an electron or muon. The integrated luminosity is 910 pb^{-1} in the e +jets channel and 870 pb^{-1} in the μ +jets channel.

A. Event Selections

The kinematic event selections are aimed at producing a pure sample of events with a leptonically decaying W boson while rejecting misidentified multijet events. Events are required to have $\cancel{E}_T > 15 \text{ GeV}$ and exactly one

isolated electron (muon) with $p_T > 15$ GeV/ c (18 GeV/ c) within $|\eta| < 1.1$ (2.0). Misidentified multijet events are suppressed by requiring that the direction of \cancel{E}_T is not aligned or anti-aligned in azimuth with the lepton or the jets. The jets are defined using a cone algorithm [8] with radius $\Delta\mathcal{R} = 0.5$. The leading jet must have $p_T > 25$ GeV/ c and the second jet $p_T > 20$ GeV/ c . Finally, the events are required to have a reconstructed primary vertex within the fiducial region of the silicon tracker with at least 3 tracks.

B. Identification of b -jets

Given the large branching fraction for the decay $H \rightarrow b\bar{b}$ for Higgs masses between 105–155 GeV/ c^2 , there is a large probability to have two b jets in the final state of a WH event. To separate the WH signal from the large W +light jets background, one or both of the jets are required to be identified by a neural network (NN) b -tagging algorithm. The variables used to identify jets originating from long-lived b hadrons rely on the presence and characteristics of a secondary vertex and tracks inside the jets which are displaced with respect to the primary interaction. We consider a jet to be tagged if it has a high NN output value; the selection requirements is set to obtain a 0.5% light-jet tag rate and 50% average efficiency in data for b jets with $|\eta| < 1.1$. To evaluate the average probability for a simulated event to be b -tagged we use parameterizations of the b -tagging efficiency derived in data.

C. Event Yields

The expected yields of $t\bar{t}$, WW , WZ , and single top events are normalized to their NLO theoretical cross sections. The multijet and W +jets backgrounds are normalized to the number of events observed in data before b -tagging has been applied. For the W +jets background, we scale the $Wb\bar{b}$ and $Wc\bar{c}$ components by a factor of 1.50 ± 0.45 to shift the leading order fraction to better represent higher order effects. This factor has been measured using data, and the large uncertainty covers the assumption that the scale factor is the same for $Wb\bar{b}$ and $Wc\bar{c}$ and the expected dependence on of the scale factor on event kinematics. The multijet background is modeled from a data sample containing non-isolated leptons. After applying all selections, the expected and observed event yields are shown in Table 1. The expected and observed distributions for lepton p_T , \cancel{E}_T and invariant mass of the two jets are shown in Appendix A for events passing all selections.

Process	e +jets channel		μ +jets channel	
	Single Tag	Double Tag	Single Tag	Double Tag
tb	6.60 ± 0.08	2.35 ± 0.03	5.10 ± 0.07	1.94 ± 0.03
tqb	11.09 ± 0.13	0.28 ± 0.01	9.08 ± 0.12	0.24 ± 0.01
$t\bar{t} \rightarrow \ell + \text{jets}$	10.86 ± 0.25	1.68 ± 0.05	6.21 ± 0.19	1.00 ± 0.04
$t\bar{t} \rightarrow \ell\bar{\ell}$	16.35 ± 0.16	5.49 ± 0.06	12.59 ± 0.14	4.61 ± 0.06
$Wb\bar{b}$	115.30 ± 2.00	15.49 ± 0.41	105.74 ± 2.04	14.79 ± 0.43
$Wc\bar{c}$	70.76 ± 1.38	1.55 ± 0.06	71.47 ± 1.36	1.50 ± 0.07
Wjj	58.29 ± 0.85	0.13 ± 0.00	55.75 ± 0.86	0.13 ± 0.00
WW	8.44 ± 0.15	0.05 ± 0.01	6.91 ± 0.13	0.04 ± 0.00
WZ	3.58 ± 0.15	0.82 ± 0.05	3.09 ± 0.12	0.65 ± 0.04
Multijets	66.24 ± 0.79	2.47 ± 0.03	25.59 ± 1.00	1.51 ± 0.06
Total Background	367.52 ± 2.73	30.30 ± 0.43	301.53 ± 2.80	26.40 ± 0.45
WH (115 GeV/ c^2)	1.02 ± 0.02	0.35 ± 0.01	0.80 ± 0.01	0.29 ± 0.01
Total Expected	368.54 ± 2.73	30.65 ± 0.43	302.33 ± 2.80	26.69 ± 0.45
Data	357	30	287	23

TABLE 1: Expected and observed number of events with exactly one b tag (Single Tag) and exactly two b tags (Double Tag). Only statistical uncertainties are shown on the expected event yields.

V. SYSTEMATIC UNCERTAINTIES

We consider two types of systematic uncertainties: uncertainties which only affect the overall normalization of the signal and background yields, and uncertainties that change the shape of kinematic al distributions.

The dominant uncertainties affecting only the overall yield come from the normalization of the $t\bar{t}$ background (18%), and the normalization of W +jets and multijets backgrounds to data together with uncertainties on the heavy flavor fraction scaling in W +jets events (17–27% on the total yield). The uncertainty on the integrated luminosity is 6%. All other systematic uncertainties affecting only the overall yield is at the few percent level or below.

The uncertainties on the jet energy scale and the tag-rate functions change the shape of kinematic distributions as well as the overall yield. The effect of these uncertainties are propagated throughout the analysis and the shape and yield differences are taken into account in the final limit setting.

VI. SEPARATION OF SIGNAL FROM BACKGROUND USING MATRIX ELEMENTS

The matrix-element-based technique attempts to make use of all the available kinematic information in the event to separate signal and background. If the vector \vec{x} represents the set of reconstructed four-momenta for all selected final state objects in the event, we define the discriminant

$$D_{WH}(\vec{x}) = \frac{P_{WH}(\vec{x})}{P_{WH}(\vec{x}) + P_B(\vec{x})}, \quad (1)$$

where $P_{WH}(\vec{x})$ is the probability that the event is coming from WH production and $P_B(\vec{x})$ is the probability that the event comes from a background process. The signal and background probability density functions of \vec{x} are computed numerically based on the normalized differential cross section for signal and background processes, respectively. Since the differential cross section for the process of interest is proportional to the matrix element squared, we call this method the ‘‘Matrix Element (ME) Method’’. We shall refer to Eq. 1 as the ‘‘ME discriminant’’.

For the signal probability, $P_{WH}(\vec{x})$, we have implemented six different matrix elements for six different values of the Higgs mass: $m_H = 105, 115, 125, 135, 145$ and $155 \text{ GeV}/c^2$. The background probability density function, $P_B(\vec{x})$, in each of the six ME discriminants is given by:

$$P_B(\vec{x}) = C_{Wbb}P_{Wbb}(\vec{x}) + C_{Wcg}P_{Wcg}(\vec{x}) + C_{Wgg}P_{Wgg}(\vec{x}) + C_{WW}P_{WW}(\vec{x}) + C_{WZ}P_{WZ}(\vec{x}) + C_{tb}P_{tb}(\vec{x}) + C_{tqb}P_{tqb}(\vec{x}), \quad (2)$$

where C_{Wbb} , C_{Wcg} , C_{Wgg} , C_{WW} , C_{WZ} , C_{tb} and C_{tqb} are, in principle, the relative fractions of each background in the data. The leading order diagrams for these processes are shown in Fig. 1. There are no explicit matrix elements used in the analysis for the multijet, $t\bar{t} \rightarrow \ell$ +jets, and $t\bar{t} \rightarrow \ell\ell$ backgrounds. That does not imply that these processes are ignored. Our background model still contains all processes and the event discriminant is computed for all of them when building the templates that will be compared to data. For the purpose of determining the values of the constants C_{bkg} in Eq. 2 we treat each of multijet, $t\bar{t} \rightarrow \ell$ +jets, and $t\bar{t} \rightarrow \ell\ell$ as being instead the most similar background for which we have an explicit matrix element. For $t\bar{t} \rightarrow \ell$ +jets and $t\bar{t} \rightarrow \ell\ell$ the most similar background is tb , while for the multijet background it is any of the Wbb , Wcg or Wgg backgrounds. The constants C_{WW} , C_{WZ} , C_{tb} and C_{tqb} are then fixed to the expected fractions according to Tab. 1. The remaining three constants (C_{Wbb} , C_{Wcg} and C_{Wgg}) are optimized for the best expected limit on the WH cross section under the constraints that all seven constants add up to unity. The optimization is done separately for each of the six Higgs mass values considered. Since the optimized values are very similar for all Higgs masses, we use the same set of values for the background constants in all six ME discriminants.

The expected and observed discriminant distributions for a Higgs mass of $115 \text{ GeV}/c^2$ are shown in Fig. 2 for single and double tagged events. The discriminant distributions for Higgs masses other than $115 \text{ GeV}/c^2$ all look very similar to the ones shown in Fig. 2.

VII. LIMIT ON THE WH CROSS SECTION

Upper limits on the rate of associated WH production with $H \rightarrow b\bar{b}$ decay as a function of Higgs boson mass are calculated using the individual per-channel ME discriminant distributions for signals, backgrounds, and data. For each discriminant distribution a total of 50 uniform bins have been used.

Limits are calculated at 95% confidence level using the semi-Frequentist CL_s approach with a Poisson log-likelihood ratio test statistic. The impact of systematic uncertainties in the shape and normalizations of the discriminant distributions is incorporated through marginalization of the Poisson probability distributions for signal and background via Gaussian distribution. All correlations in systematic uncertainties are maintained. The expected distributions for

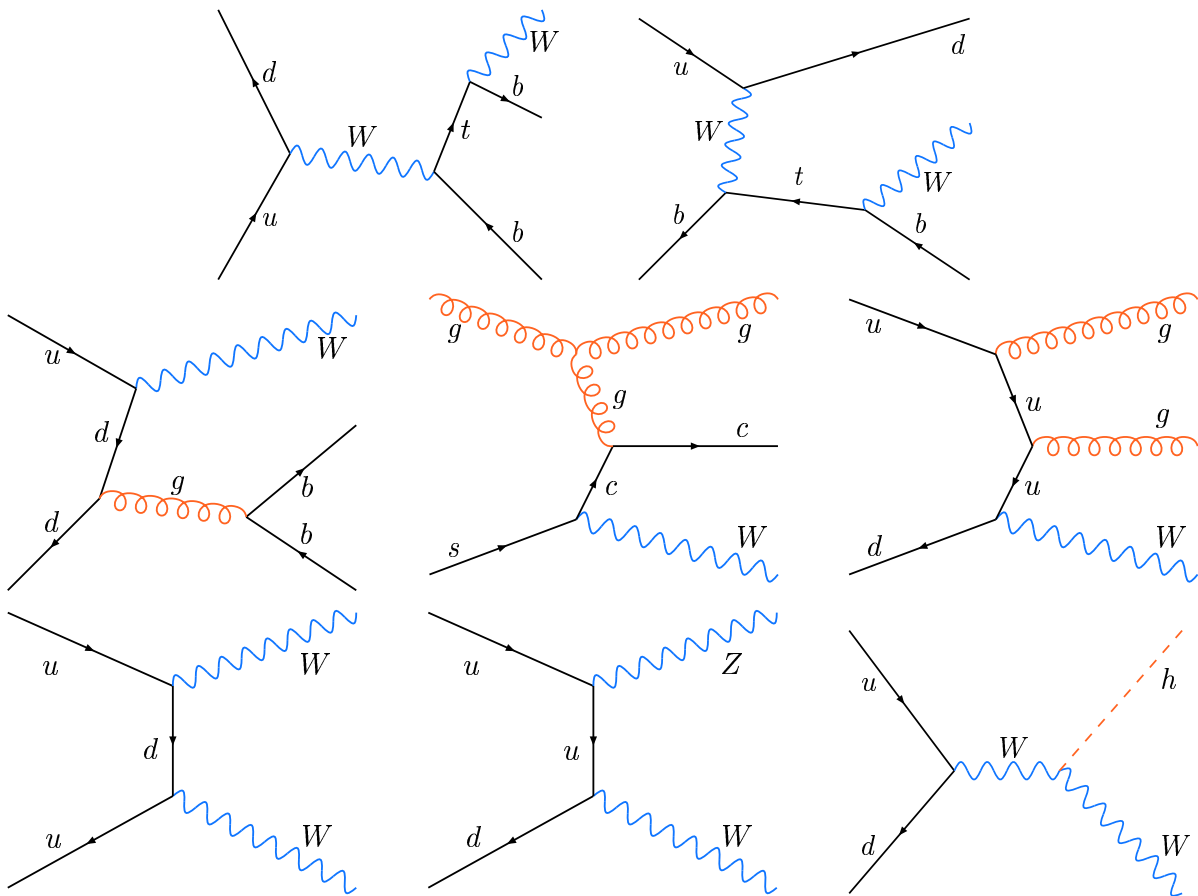


FIG. 1: Representative Feynman diagrams corresponding to the leading-order matrix elements used for event probability calculation. Upper row: $ud \rightarrow tb$, $ub \rightarrow td$; Middle row: $ud \rightarrow Wbb$, $sg \rightarrow Wcg$, $ud \rightarrow Wgg$. Lower row: $uu \rightarrow WW$, $ud \rightarrow WZ$, $ud \rightarrow WH$.

background are evaluated by minimizing a profile likelihood function, referencing the shape and rate of the observed distributions. All derived upper limits are calculated with an accuracy of 0.1%: *i.e.*, $94.9\% \leq CL_s \leq 95.1\%$.

The expected and observed limits on $\sigma_{WH} \times BR(H \rightarrow b\bar{b})$ for a combination of all four channels (e +jets and μ +jets, single and double tagged) is shown in Fig. 3. The limits are shown as the ratio of the expected limit over the standard model prediction. Table 2 gives numerical values for the expected and observed limits for a few selected values of the Higgs boson mass.

$\sigma_{WH} \times BR(H \rightarrow b\bar{b})$ limit (95% CL)		
m_H [GeV/ c^2]	Expected	Observed
105	≤ 1.40 pb	≤ 2.17 pb
115	≤ 1.20 pb	≤ 1.74 pb
125	≤ 1.13 pb	≤ 1.52 pb
135	≤ 0.93 pb	≤ 1.05 pb
145	≤ 0.84 pb	≤ 0.75 pb

TABLE 2: Expected and observed limit on $\sigma_{WH} \times BR(H \rightarrow b\bar{b})$ for a few selected values of the Higgs boson mass.

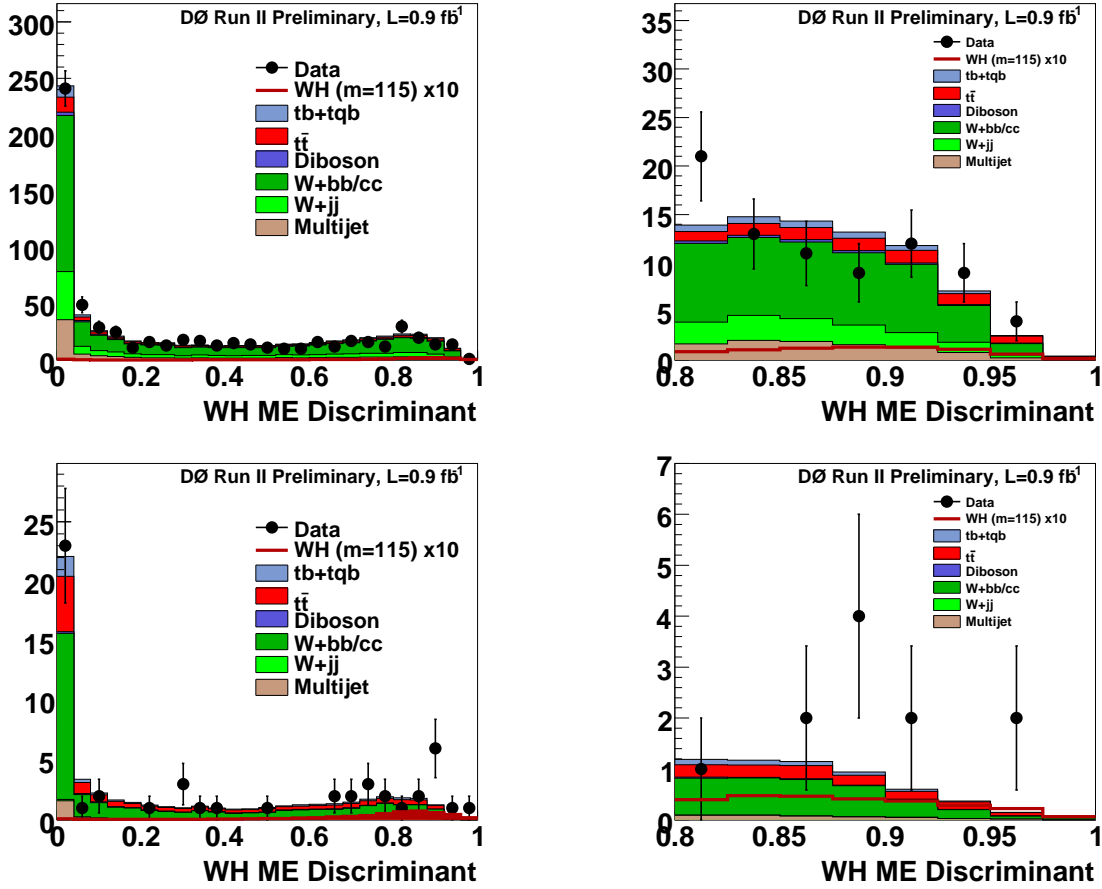


FIG. 2: Discriminant plots for a Higgs mass of $115 \text{ GeV}/c^2$ in $e+\mu$ channel with two jets for: Upper row: equal one tag; lower row: equal two tags. Left column: full output range; right column: close-up of the high end of the distributions.

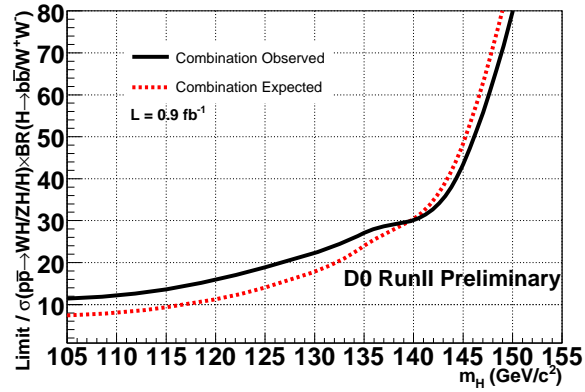


FIG. 3: Expected and observed limit on the $\sigma_{WH} \times BR(H \rightarrow b\bar{b})$ cross section for a combination of all four channels: e +jets single tagged, e +jets double tagged, μ +jets single tagged and μ +jets double tagged. The expected limits is shown as the ratio of the expected limit over the standard model prediction.

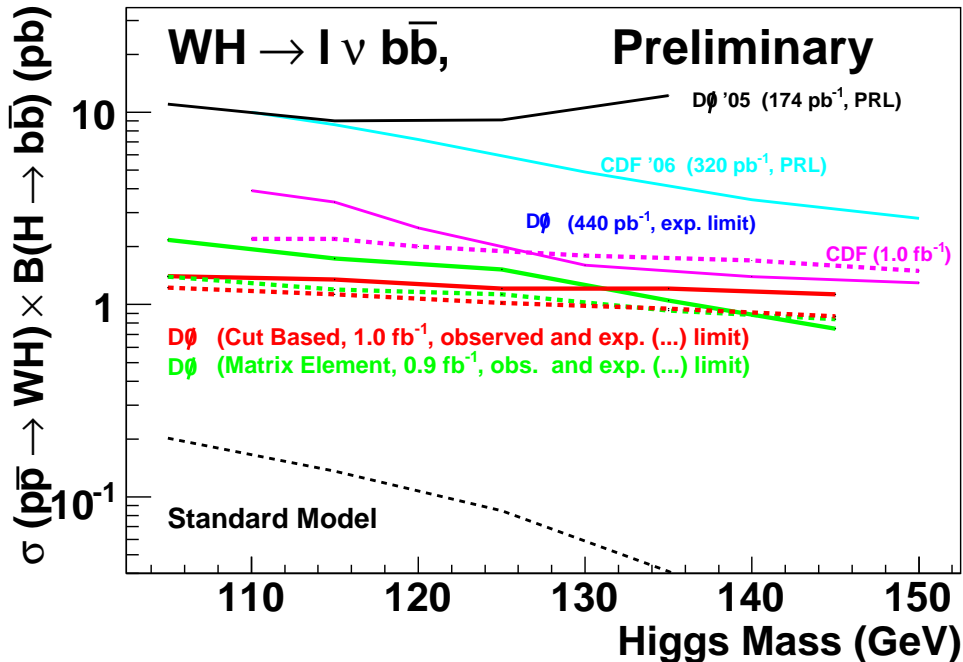


FIG. 4: The expected (dashed green curve) and observed (solid green curve) limit on $\sigma_{WH} \times BR(H \rightarrow b\bar{b})$ for the matrix element analysis compared with other measurements from CDF and DØ.

VIII. SUMMARY

We have used leading-order matrix elements to separate the expected WH signal from the background. This analysis uses lepton+jets events selected from approximately 900 pb^{-1} of Run IIa data. The WH discriminants are used to set an upper limit on the WH cross section as a function of the Higgs boson mass. For a Higgs boson mass of $115 \text{ GeV}/c^2$ we arrive at a 95% CL upper limit of:

$$\sigma_{WH} \times BR(H \rightarrow b\bar{b}) \leq 1.74 \text{ pb} \quad (\leq 1.20 \text{ pb expected}).$$

Figure 4 compares the obtained limit for the WH cross section with previous measurements from CDF and DØ.

Acknowledgments

We thank the staffs at Fermilab and collaborating institutions, and acknowledge support from the DOE and NSF (USA); CEA and CNRS/IN2P3 (France); FASI, Rosatom and RFBR (Russia); CAPES, CNPq, FAPERJ, FAPESP and FUNDUNESP (Brazil); DAE and DST (India); Colciencias (Colombia); CONACyT (Mexico); KRF and KOSEF (Korea); CONICET and UBACyT (Argentina); FOM (The Netherlands); PPARC (United Kingdom); MSMT (Czech Republic); CRC Program, CFI, NSERC and WestGrid Project (Canada); BMBF and DFG (Germany); SFI (Ireland); The Swedish Research Council (Sweden); Research Corporation; Alexander von Humboldt Foundation; and the Marie Curie Program.

-
- [1] S. Abachi *et al.*, Nucl. Instrum. Methods Phys. Res. A **338**, 185 (1994).
[2] DØ Collaboration, V. Abazov *et al.*, “The Upgraded DØ Detector”, Nucl. Instr. and Methods A **565**, 463 (2006).
[3] T. Sjöstrand *et al.*, “PYTHIA 6.2: Physics and Manual,” hep-ph/0108264. We used version 6.323.
[4] D.J. Lange, “The EvtGen Particle Decay Simulation Package,” Nucl. Instrum. Meth. A **462**, 152 (2001). We used version 00.00.17.

- [5] M.L. Mangano *et al.*, “ALPGEN, a Generator for Hard Multiparton Processes in Hadronic Collisions,” J. High Energy Phys. **0307**, 001 (2003). We used ALPGEN version 2.05.
- [6] E.E. Boos *et al.*, “Method for Simulating Electroweak Top-Quark Production Events in the NLO Approximation: SingleTop Generator,” Phys. Atom. Nucl. **69**, 1317 (2006).
- [7] J. Pumplin *et al.*, “New Generation of Parton Distributions with Uncertainties from Global QCD Analysis,” J. High Energy Phys. **0207**, 012 (2002). We used version CTEQ6L1.
- [8] G. C. Blazey *et al.*, in *Proceedings of the Workshop on QCD and Weak Boson Physics in Run II*, 1999, edited by U. Baur, R. K. Ellis and D. Zeppenfeld, Fermilab-Pub-00/297, p. 47.

APPENDIX A: KINEMATIC DISTRIBUTIONS OF SELECTED EVENTS

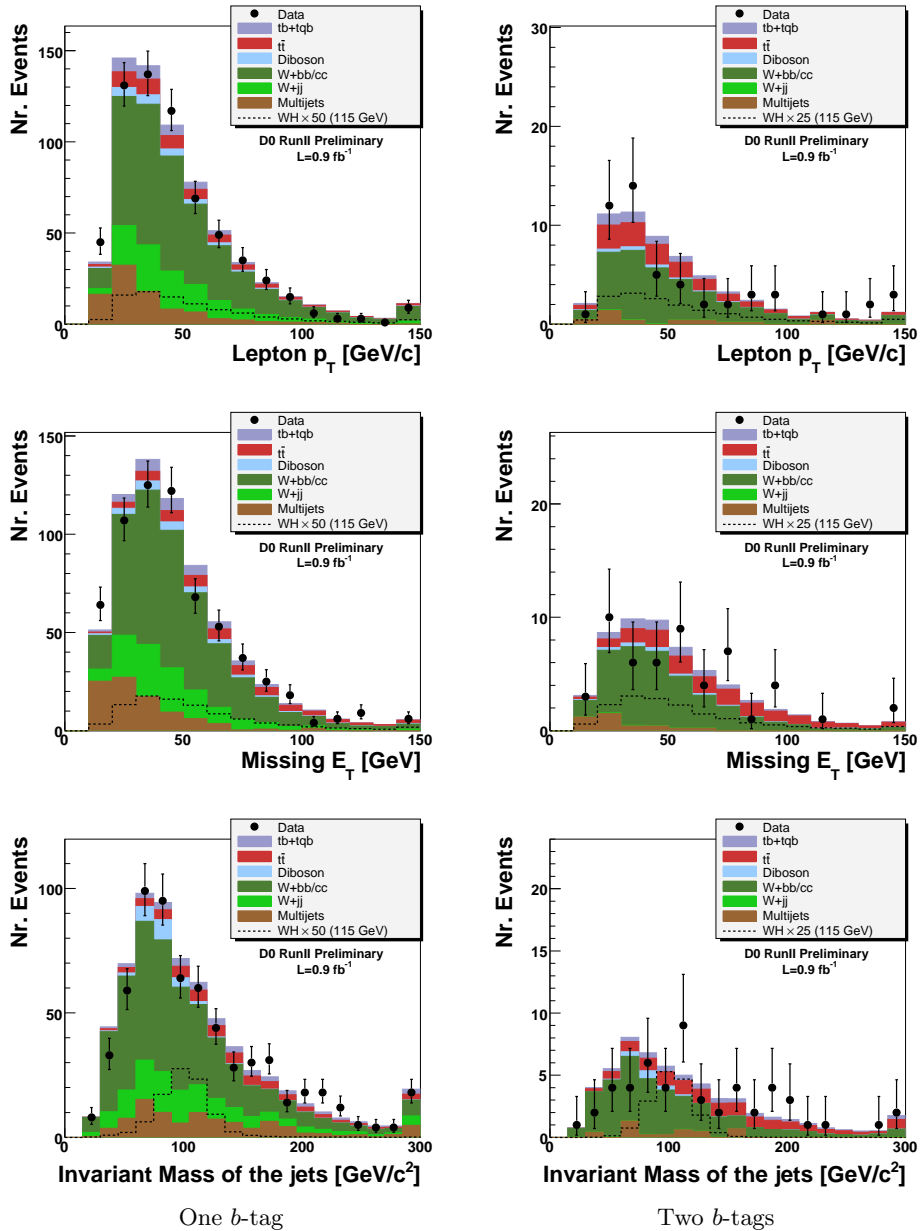


FIG. 5: Kinematic distributions for events which passes the full selection. Left column shows events events with exactly one b -tagged jet and right column shows events with two b -tagged jets.